Available online at www.sciencedirect.com
ScienceDirect
Journal of Sound and Vibration 310 (2008) 230–242
JOURNAL OF SOUND AND VIBRATION
www.elsevier.com/locate/jsvi

Nonlinear longitudinal/transversal modal interactions in highly extensible suspended cables

Narakorn Srinil, Giuseppe Rega*

Department of Structural and Geotechnical Engineering, Sapienza University of Rome, via A. Gramsci, Rome 00197, Italy

Received 24 October 2006; received in revised form 28 July 2007; accepted 30 July 2007
Available online 14 September 2007

Abstract

Recent research literature mostly deals with nonlinear resonant dynamics of low-extensible cables involving transversal modes. Herein, we aim to investigate geometrically nonlinear longitudinal/transversal modal interactions in highly extensible suspended cables, whose material properties are assumed to be linearly elastic. Depending on cable elasto-geometric properties, the spectrum of low-order planar frequencies manifests primary and secondary frequency crossover phenomena of transversal/transversal and longitudinal/transversal modes, respectively. By focusing on 1:1 internal resonances, nonlinear equations of finite-amplitude, harmonically forced and damped, cable motion are considered, fully accounting for overall inertia and displacement coupling effects. Meaningful quadratic nonlinear contributions of non-resonant, higher-order, longitudinal modes are highlighted via a multimode-based, second-order multiple scales solution. Overall coupled/uncoupled dynamic responses, bifurcations, stability and space–time-varying displacements due to longitudinal/transversal (vs. transversal/transversal) modal interactions at secondary (vs. primary) crossovers are analytically and numerically evaluated, along with the resonant longitudinal mode-induced dynamic forces.

1. Introduction

Suspended cables are basic structural components widely used in civil, mechanical, electrical and offshore ocean engineering. Cables with high extensibility or elongation, reaching large initial strain without undergoing failure in tension, are often found, for instance, in automotive industry including antennae, cable–crane systems and connections to control panels, or in oceanographic applications such as tethered buoys and moorings. Depending on the material and mechanical properties, highly extensible cables offer great flexibility and advantages over low-extensible cables in some technical applications that require long-span structural elements having the capability to withstand excessive dynamic stresses.

Low-extensible, e.g. metallic, suspended cables are characterized by high values of Young's modulus giving rise to small initial static strain. The transversal displacements substantially dominate their low-order modes, whereas the corresponding first longitudinal mode (also known as elastic mode)—characterized by a prevailing longitudinal displacement—usually occurs at a relatively higher-order frequency [1–3] along the

*Corresponding author. Tel.: +39 06 49919195; fax: +39 06 49919192.
E-mail addresses: narakorn.srinil@uniroma1.it (N. Srinil), giuseppe.rega@uniroma1.it (G. Rega).

0022-460X/$ - see front matter © 2007 Elsevier Ltd. All rights reserved.
doi:10.1016/j.jsv.2007.07.056

so-called "elastic mode transition" line, which has been discussed originally in Ref. [1] and more recently in Ref. [3]. In the case of *highly extensible*, e.g. synthetic, cables, the first longitudinal mode and its modal transition occur, on the contrary, at a much lower-order (e.g., 3rd or 4th) frequency [4]. Triantafyllou and Yue [5] analyzed the effect of hysteretic damping and large sensitivity to parametric changes in linear vibration of synthetic cables.

Many theoretical studies have investigated nonlinear vibrations of low-extensible suspended cables involving different kinds of internal resonances of transversal modes [6]. For such systems, the influence of longitudinal inertia and the associated higher-order coupling of longitudinal/transversal displacements are often neglected through the kinematic condensation procedure, which assumes cable quasi-static stretching entailing spatially independent dynamic strain [7]. Accordingly, this simplified model may lead to significant quantitative and/or qualitative discrepancies in the nonlinear internally resonant responses and stress estimations of even shallow cables [8]. As a matter of fact, using the condensed model in the analysis of longitudinal modes (or transversal modes with significant longitudinal components) for highly extensible (or low-extensible non-shallow) cables would be meaningless. Based on a numerical finite difference scheme accounting for longitudinal inertia, Newberry and Perkins [9] investigated the resonant tensioning mechanism in low-extensible submerged cables due to a 3:1 internal resonance of high-order longitudinal/transversal (85th/28th) modes, and observed strong energy transfer between these coupled modes. The nonlinear forced responses of highly extensible underwater cables subject to current fluid forces were studied in Ref. [10] implementing a nonlinear stress–strain relationship.

The objective of this analytical–numerical study is to complement previous investigations of nonlinear modal interactions of low-extensible cables [8,11] by qualitatively comparing typical *transverse/transverse* interactions at 1:1 internal resonances with the companion *longitudinal/transversal* interactions mostly occurring in highly extensible cables. In view of such a comparison, the same non-condensed model and linearly elastic material properties as of low-extensible cables are considered, although the latter assumption might be questionable from a modeling standpoint. Within this framework, (i) the geometrically quadratic nonlinear effect of higher-order longitudinal modes on a second-order multiple scales solution is highlighted and (ii) insight into dynamic interaction features involving *low-order* longitudinal/transversal resonant modes is gained. The first issue addresses a meaningful aspect from a practical reduced-order modeling viewpoint with respect to low-extensible cables [8], whereas the second issue is discussed against the case involving interaction of only transverse modes. Both numerical continuation and direct time integration of system modulation equations are performed, verifying the obtained responses and illustrating the existence of periodic and aperiodic oscillations involving longitudinal modes. For the sake of completeness, the corresponding space- time-varying nonlinear dynamic displacements and tensions are also examined.

2. Equations of motion and elastic mode transition

With reference to the Cartesian coordinates in Fig. 1a, nonlinear finite-amplitude planar vibration about the static equilibrium of a highly extensible, small-sagged, suspended cable subject to a uniformly distributed transversal harmonic excitation is governed by an infinite series of ordinary-differential equations expressed in non-dimensional state-space form as [8]

$$\begin{aligned}&\dot{f}_m - p_m = 0,\\ &\dot{p}_m + 2\mu_m p_m + \omega_m^2 f_m = \sum_{i=1}^{\infty}\sum_{j=1}^{\infty} \Lambda_{mij} f_i f_j + \sum_{i=1}^{\infty}\sum_{j=1}^{\infty}\sum_{k=1}^{\infty} \Gamma_{mijk} f_i f_j f_k + \left(F\int_0^1 \varphi_m \,\mathrm{d}x\right)\cos\,\Omega t\end{aligned} \tag{1}$$

for $m = 1, 2, \ldots, \infty$, wherein the quadratic and cubic nonlinear coefficients read

$$\Lambda_{mij} = -\alpha \int_0^1 \frac{1}{\left(1+y'^2\right)^{3/2}} \left\{ \phi'_m \left(\frac{3}{2}\phi'_i\phi'_j + y'\phi'_i\varphi'_j + \frac{1}{2}\varphi'_i\varphi'_j \right) + \varphi'_m \left(\frac{y'}{2}\phi'_i\phi'_j + \phi'_i\varphi'_j + \frac{3}{2}y'\varphi'_i\varphi'_j \right) \right\} \mathrm{d}x, \tag{2}$$

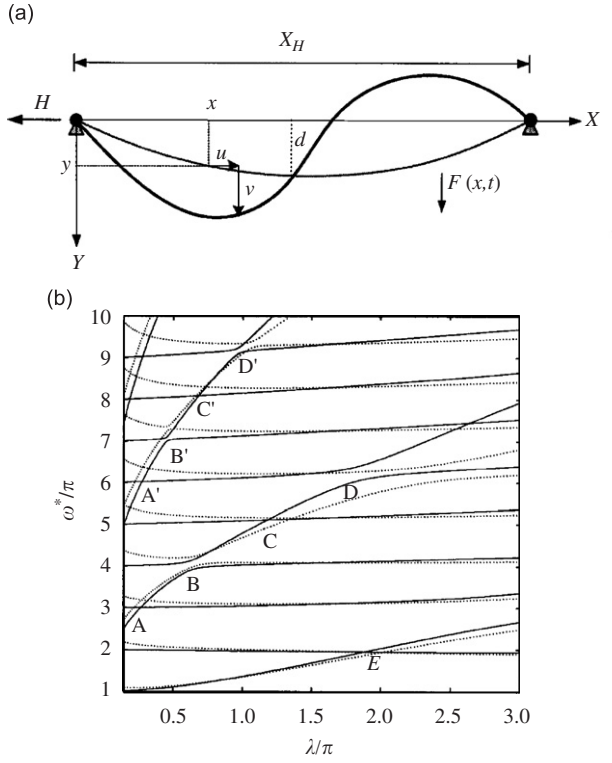

Fig. 1. (a) The planar model of a highly extensible suspended cable. (b) Natural frequency spectrum and associated primary/secondary crossover phenomena: solid (dotted) lines denote sine series-based (finite element) results of approximate (exact) model.

$$\Gamma_{mijk} = -\frac{\alpha}{2}\int_0^1 \frac{1}{\left(1+y'^2\right)^{3/2}}\left\{\phi'_m\left(\phi'_i\phi'_j\phi'_k + \phi'_i\varphi'_j\varphi'_k\right) + \varphi'_m\left(\phi'_i\phi'_j\varphi'_k + \varphi'_i\varphi'_j\varphi'_k\right)\right\}\mathrm{d}x. \tag{3}$$

f_m (p_m) are time-dependent generalized displacement (velocity) modal coordinates, related to the longitudinal (or horizontal) u and transversal v motion of original system through $U^J = \sum_{m=1}^{\infty} f_m \zeta_m^J$, $V^J = \sum_{m=1}^{\infty} p_m \zeta_m^J$, $J = 1, 2$, with $U^1 = u$, $U^2 = v$, $V^1 = \dot{u}$, $V^2 = \dot{v}$, $\zeta_m^1 = \phi_m$, $\zeta_m^2 = \varphi_m$ being the relevant linear u and v orthonormalized eigenfunctions, and ω_m being natural frequencies. The parameters are μ_m damping, $F(\Omega)$ the variable amplitude (frequency) of excitation, $\alpha = E_C A_C/H$ with E_C being the cable Young's modulus, A_C the uniform cross-sectional area and H the constant horizontal static tension. The static configuration under its own weight is assumed as an inextensible parabola $y \approx 4dx(1-x)$ [7], with d being the cable sag-to-span ratio. In Eq. (1), $x(t)$ is the space (time) independent variable and the prime (dot) denotes the associated derivative. The space-related variables have been non-dimensionalized with respect to the cable span X_H, whereas the time-related variables have been non-dimensionalized with respect to the characteristic time $X_H\sqrt{w_C/gH}$, with g being the gravity and w_C the cable self-weight per unit unstretched length. Zero displacements at hinged–hinged boundaries are considered.

It is worth remarking that Eq. (1) explicitly accounts for overall inertia and u/v displacement coupling effects, and captures geometrically quadratic (2) and cubic (3) nonlinearities due to cable sag and axial extensibility. As in low-extensible cable cases, the initial static strain (e) has been assumed such that $(1+e) \approx 1$, an assumption to be further verified. However, the arbitrary spatial/temporal variation of dynamic strain is accounted for in Eq. (1) [8,12]. Associated natural frequencies and modal shape functions are obtained based on admissible sine series of linear u/v displacements and the Galerkin approach [12]. The overall cable dynamics depends on the well-known elasto-geometric parameter $\lambda/\pi = (1/\pi)\sqrt{(w_C S_C)^2 E_C A_C/H^3}$ [1,7],

in which S_C is the cable equilibrium length. To suitably discuss the geometrical nonlinear effect of possibly low-order longitudinal modes on dynamic response (Section 4), we consider a suspended cable having linearly elastic material properties, however with a low axial rigidity $E_C A_C$ chosen, along with the other parameters, in such a way to produce a range of very low λ/π values. Of course, these are representative of an extremely soft material. By varying H, and thus S_C, the spectrum of the first 12 frequencies ω^*/π, normalized with respect to the characteristic time $S_C\sqrt{w_C/gH}$ [1], is plotted vs. λ/π in Fig. 1b, which refers to different sagged and strained cables. Solid lines denote results with 40 sine series, whereas dotted lines are corresponding finite element (FE) results—utilized to validate the approximate cable model—of the more realistic linearized model [12] accounting for 50 beam elements, extensible catenary static profile and space-varying $(1+e)$ effect.

Quantitative discrepancies are seen to occur mostly in some higher-frequency results both at low (e.g., regions A′–D′) and higher (e.g., region D) λ/π values. Such differences between the two cable model predictions are particularly concerned with the static equilibrium solution, whose different assumptions on the initial static strain are likely to affect the frequency values, as well as the possible shift of λ/π (e.g., region D) due to different ensuing values of (inextensible vs. extensible) equilibrium length S_C. Of course, the discrepancies also depend on the differences in the Galerkin-based spatial discretization procedure, i.e. the number of terms in sine-based series vs. the number of FEs, of the two considered solution techniques. Nevertheless, overall qualitative agreement occurs between the results of the two models, both exhibiting a "primary" frequency crossover E as in the low-extensible (higher E_C) cable case [7]. Moreover, both models reveal a sequence of "secondary" frequency crossover phenomena A, C, etc.—spaced out with frequency avoidance phenomena B, D, etc.—as it typically happens at higher-order modes of low-extensible cables [1,3]. This sequence highlights the coexistence of a "first elastic mode transition" occurring at low-order modes [4] and provides information on possible relevant 1:1 (and other) internal resonances. A second elastic mode transition and so on consecutively occurs at higher-order frequencies, e.g., the A′–D′ sequence.

By way of examples, internally 1:1 resonant cables at crossovers A, C and E are considered, whose relevant parameters, frequencies of low-order (ω_r) and high-order (ω_s) modes are given in Table 1. The associated (r, s) shape functions are displayed in Fig. 2. It is found that—due to the first elastic mode transition at low (A) or higher (C) order frequencies—one (r) of the coalescing frequencies of *both* cables A (solid lines) and C (dashed lines) corresponds to the *first longitudinal* mode with predominant symmetric u and smaller anti-symmetric v amplitudes, whereas the coexisting higher s frequencies correspond to symmetric transversal modes having different predominant symmetric v (very small anti-symmetric u) amplitudes. On the other hand, both the low/high coalescing frequencies of cable E (dotted lines) correspond to transversal modes being anti-symmetric and symmetric, respectively.

As regards Fig. 1b, the maximum percent value of the space-varying initial static strain e from FE analysis is about 12.6% for cable A and 4% for cable E, the latter corresponding to the string/inextensible cable transition [4,7]. This means that the $(1+e)$ term plays a greater role in cable A than in cable E. Yet, by comparing the first 12 frequencies (Fig. 1b) associated with the two models for cable A, it is found that the maximum percent difference of frequencies with respect to the FE-based model is about 5.84%, thus being acceptable. Accordingly, the assumption $(1+e)\approx 1$ made in the sine-based eigenvalue problem may be plausible for the considered sag and extensibility (λ/π) range in which cables A ($d\approx 0.038$) and E ($d\approx 0.134$) exhibit largest (smallest) and smallest (largest) e (sag), respectively.

Table 1
Given parameters and properties of different primary/secondary crossover cables

Cable	λ/π	d	r–s		ω_r	ω_s
			Order	Mode[a]		
A	0.27	0.038	3–4	u–v	9.403	9.408
C	1.17	0.099	5–6	u–v	15.616	15.648
E	1.88	0.134	1–2	v–v	5.866	5.869

[a] $u(v)$ denotes dominant longitudinal (transverse) mode.

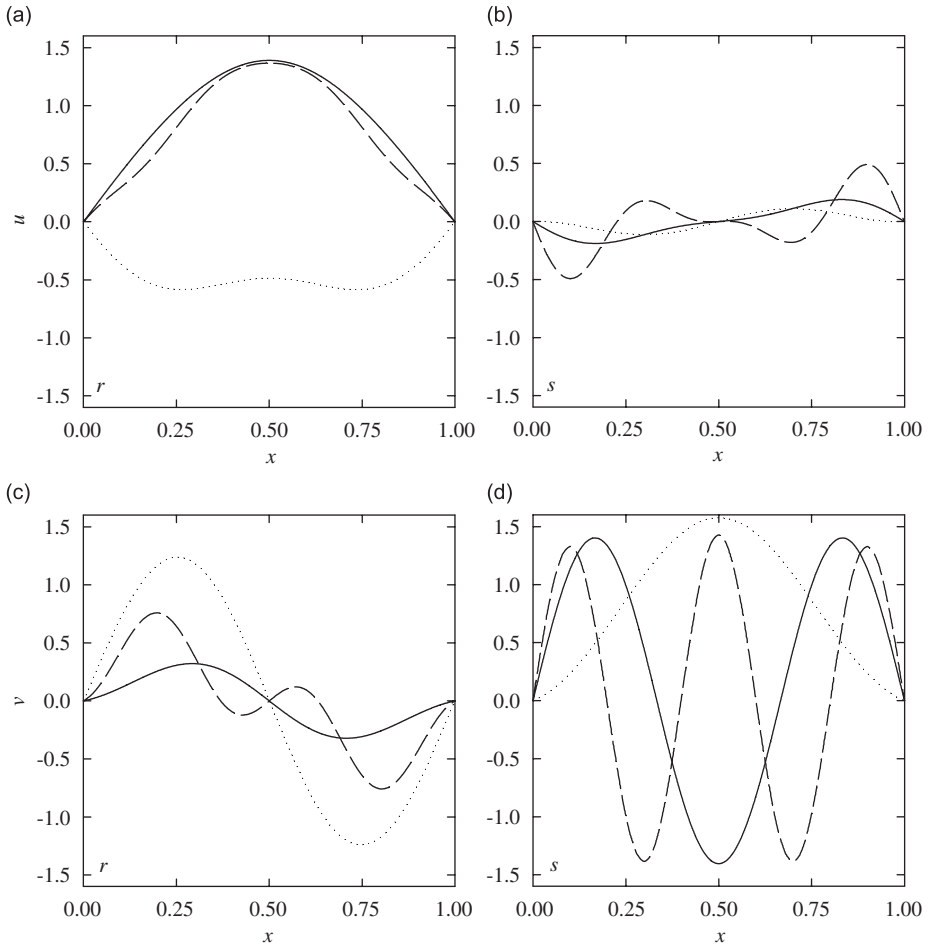

Fig. 2. u and v displacements of low- and high-frequency (r, s) modes: solid (dashed, dotted) lines denote cable A (C and E) in Table 1.

As a further remark, similar elastic mode transitions may take place for highly extensible inclined cables, with both the primary and secondary crossovers (involving symmetric/anti-symmetric modes) in Fig. 1b being replaced with frequency avoidances or veering (involving hybrid or asymmetric modes) because of the asymmetry of inclined configurations [1,13]. Here, based on the Cartesian reference frame, we only deal with horizontal cables as their longitudinal (i.e., horizontal) and transversal (i.e., vertical) mode shapes are clearly distinguished from each other. Yet, in addressing some modal interaction features of highly extensible inclined cables, it might be preferable to use the arc-length or space-varying local coordinates [1,9] in discriminating actual longitudinal (i.e., tangential to the cable axis) modes from transversal (i.e., normal to the cable axis) modes since the Cartesian coordinates generally entail commensurate horizontal/vertical displacements depending upon the cable inclination [14].

3. Modulation equations and longitudinal modal contributions

Even if no external force is supplied in the u direction, energy from the directly excited transversal mode is transferred to the longitudinal mode through a 1:1 internal resonance. Primary resonance of a high-frequency transversal s mode (Fig. 2) is considered. Based on a full-eigenbasis Galerkin discretization and a second-order multiple scales solution of Eq. (1), real-valued modulation equations, describing the nonlinear interaction of

amplitudes (a_r, a_s) and phases (β_r, β_s) of the two 1:1 resonant (r, s) modes, are obtained, in polar form, as [8]

$$\dot{a}_r = -\mu_r a_r + \frac{K a_s^2 a_r \sin 2\Delta}{8\omega_r}, \tag{4}$$

$$a_r\dot{\gamma}_r = (\sigma_f + \sigma)a_r + \frac{K_{rr}a_r^3}{8\omega_r} + \frac{K_{rs}a_r a_s^2}{8\omega_r} + \frac{K a_s^2 a_r \cos 2\Delta}{8\omega_r}, \tag{5}$$

$$\dot{a}_s = -\mu_s a_s - \frac{K a_r^2 a_s \sin 2\Delta}{8\omega_s} + \frac{1}{2\omega_s} F \int_0^1 \varphi_s \,\mathrm{d}x \sin\gamma_s, \tag{6}$$

$$a_s\dot{\gamma}_s = \sigma_f a_s + \frac{K_{ss}a_s^3}{8\omega_s} + \frac{K_{rs}a_s a_r^2}{8\omega_s} + \frac{K a_r^2 a_s \cos 2\Delta}{8\omega_s} + \frac{1}{2\omega_s} F \int_0^1 \varphi_s \,\mathrm{d}x \cos\gamma_s, \tag{7}$$

where $\gamma_r = (\sigma_f+\sigma)t-\beta_r$, $\gamma_s = \sigma_f t-\beta_s$, $\Delta = \gamma_r-\gamma_s$ are relative phases, σ_f and σ are external and internal detuning parameters described through $\Omega = \omega_s+\varepsilon^2\sigma_f$, $\omega_s = \omega_r+\varepsilon^2\sigma$, respectively, with ε being a bookkeeping parameter. Let σ_f or F be the system varying control parameter, Eqs. (4)–(7) reveal both uncoupled-mode ($a_r = 0$, $a_s \neq 0$) and coupled-mode ($a_r \neq 0$, $a_s \neq 0$) solutions. The effective second-order coefficients, accounting for an infinite-dimensional series of resonant (quadratic/cubic) and non-resonant (quadratic) modes (nonlinearities), read [8]

$$K_{hh} = \sum_{m=1}^{\infty}\left[(\Lambda_{hhm}+\Lambda_{hmh})\Lambda_{mhh}\left(\frac{2}{\omega_m^2}+\frac{1}{\omega_m^2-4\omega_h^2}\right)\right] + 3\Gamma_{hhhh}, \quad h = r,s, \tag{8}$$

$$K_{rs} = \sum_{m=1}^{\infty}\left[(\Lambda_{rrm}+\Lambda_{rmr})\frac{2\Lambda_{mss}}{\omega_m^2} + (\Lambda_{rsm}+\Lambda_{rms})(\Lambda_{mrs}+\Lambda_{msr})\left(\frac{1}{\omega_m^2-(\omega_s+\omega_r)^2}+\frac{1}{\omega_m^2-(\omega_s-\omega_r)^2}\right)\right] + 2(\Gamma_{rssr}+\Gamma_{rsrs}+\Gamma_{rrss}), \tag{9}$$

$$K = \sum_{m=1}^{\infty}\left[(\Lambda_{ssm}+\Lambda_{sms})\frac{\Lambda_{mrr}}{\omega_m^2-4\omega_r^2} + \frac{(\Lambda_{srm}+\Lambda_{smr})(\Lambda_{mrs}+\Lambda_{msr})}{\omega_m^2-(\omega_s-\omega_r)^2}\right] + \Gamma_{srrs}+\Gamma_{srsr}+\Gamma_{ssrr}. \tag{10}$$

Based on Eqs. (2) and (3), these coefficients depend, in general, on contributions of the cable elasto-geometric parameter, sag, spatial modal characteristics (e.g., Fig. 2) and system frequency relationship. Thus, based on a finite number of retained modes, overall coefficients affect nonlinear response through Eqs. (4)–(7). Apart from the effective cubic coefficients which depend on solely resonant (r,s) modes, the percentage (C^m) of each m modal contribution (K^{qm}) to the effective quadratic coefficients ($K^q_{rr}, K^q_{ss}, K^q_{rs}, K^q$) in Eqs. (8)–(10) is evaluated [8,11] through $C^m = \left(K^{qm}\Big/|\sum_{m=1}^{M}K^{qm}|\right)\times 100$, in which M is the number of retained modes. The absolute of the denominator implies that one also accounts for whether each modal contribution produces a softening or hardening effect, and entails the overall sum $\sum C^m$ to be either 100 or -100%. A second-order closed-form solution of 1:1 resonant u/v dynamic configurations—depending on coupled amplitudes, relative phases and spatial profile corrections due to quadratic nonlinearities of every retained mode—is given in Refs. [8,14].

With reference to Table 1 and Figs. 1 and 2, the percentage C^m values of quadratic contribution from each resonant (underlined) and non-resonant mode to coefficients (9)–(11) are compared between cables A and E in Table 2, with $M = 25$ and 40, respectively. With the analysis of low-extensible cables at primary crossovers in the background [8], here we discuss and distinguish between the longitudinal/transversal and transversal/transversal modal interactions of highly extensible cables at secondary (A) and primary (E) crossovers, respectively. It is found that since both cables A and E, as well as C, involve r/s interactions between symmetric/anti-symmetric u (anti-symmetric/symmetric v) displacements (see Fig. 2), the nonlinear orthogonality properties (do not) affect the coefficients with (mixed) symmetric or anti-symmetric modal-based eigenfunctions [8] of both highly extensible cables. This entails that, particularly at low-frequency order,

Table 2
A comparison of modal contributions to second-order quadratic coefficients of cables A and E

m	K^q_{rr}		K^q_{ss}		K^q_{rs}		K^q	
	A	E	A	E	A	E	A	E
1	2.311	0	5.286	0	7.057	28.108	−0.063	93.631
2	0	39.582	0	88.896	71.798	47.220	47.695	−17.507
3	0	0.052	0	1.324	0.923	−1.691	0.806	3.375
4	0.412	0	0.793	0	1.363	4.516	−0.133	0.889
5	0	1.535	0	0.645	16.074	−0.307	48.054	−0.783
6	−0.101	0	−0.020	0	0.622	6.615	−0.416	5.444
7	**−102.729**	0	−0.092	0	−0.173	6.079	3.821	5.231
⋮	⋮	⋮	⋮	⋮	⋮	⋮	⋮	⋮
11	0	0	0	0	0.756	0	0.156	0
12	0.015	0.063	0.003	0	−0.007	−0.006	−0.004	−0.007
13	0	0.500	0	0.054	0	0.070	0	0.087
⋮	⋮	⋮	⋮	⋮	⋮	⋮	⋮	⋮
19	0	0	0	0	2.156	**14.638**	0.573	**15.854**
⋮	⋮	⋮	⋮	⋮	⋮	⋮	⋮	⋮
23	0.012	0	**93.927**	0	−1.334	0.008	−0.438	0.008
24	0	0.045	0	0	0	−0.006	0	−0.007
25	0	0	0.012	0	0	0.004	0	0
26		**57.518**		**8.823**		**−9.868**		**−11.272**
⋮		⋮		⋮		⋮		⋮

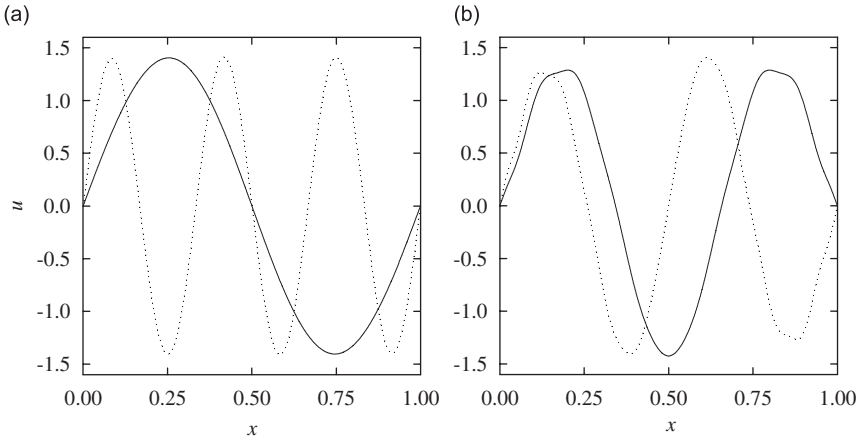

Fig. 3. u displacements of high-order elastic modes of cables (a) A and (b) E: solid lines denote (a) 7th and (b) 19th modes; dotted lines denote (a) 23rd and (b) 26th modes.

both symmetric and anti-symmetric transversal modes contribute to K^q_{rs}, K^q, whereas only symmetric transversal modes, e.g., $m = 6$ (5) for cable A (E), contribute to K^q_{rr}, K^q_{ss}.

Generally speaking, the two cables highlight significant quadratic contributions from non-resonant, besides resonant, modes. However, while contributions from resonant transversal modes play a significant role for cable E, those from resonant longitudinal/transversal modes are nearly negligible for cable A. This highlights how such resonant modes play a role only in the associated cubic coefficients in Eqs. (8)–(10). Indeed, the most outstanding quadratic contributions of cable A come from non-resonant longitudinal (higher-order) modes (bold), see, for example, the second longitudinal mode ($m = 7$) in K^q_{rr} and the sixth longitudinal mode ($m = 23$) in K^q_{ss}, whose predominant u displacements are both anti-symmetric, as depicted in Fig. 3a. Note that the non-resonant transverse lower-order (e.g., $m = 2$, 5) modes also give meaningful contributions to K^q_{rs} and

K^q. In turn, cable E reveals significant contributions from longitudinal higher-order modes, too, e.g., with $m = 19$ (K^q_{rs}, K^q) and $m = 26$ (all coefficients), whose predominant u displacements are symmetric and anti-symmetric, respectively, as shown in Fig. 3b. Since the values of associated frequency factor terms in Eqs. (8)–(10) are small, i.e., of the order of $O(10^{-1})$–$O(10^{-4})$, there is no diverging effect possibly due to a higher-order planar internal resonance [15].

Therefore, overall analyses highlight significant higher-order longitudinal modal contributions for both primary/secondary crossover cables having high extensibility, with special emphasis on the latter. The associated effects are likely to increase with cable sag due to the occurrence of consecutive elastic mode transitions giving rise to coexisting higher-order longitudinal modes. This gives us clear hints about the insufficient minimal-order model accounting for only resonant modes and the need to use reduced-order models of highly extensible cables with more degrees of freedom, up to a properly detected (minimum) frequency order, than those of lower-extensible cables at primary first or second crossover, where lower-order transversal modes are sufficiently accounted for in the same 1:1 resonant solution [8]. In the following, to obtain solution convergence, higher-order non-resonant—symmetric as well as anti-symmetric—longitudinal modes are accounted for.

4. Longitudinal/transversal modal interactions

Retaining the first 25, 32 and 40 modes for cables A, C and E, respectively, the pertinent second-order coefficients, incorporating quadratic and cubic nonlinearities, are comparatively given in Table 3. Overall, 1:1 resonances are activated as $K \neq 0$ [8], and there are quantitative and/or some qualitative differences observed in their values and/or sign, which would certainly affect modal interaction features of different sagged cables, see, e.g., K_{rr} and K_{ss}. Based on the Cartesian form [14] of Eqs. (4)–(7) via the transformations $a_i = (p_i^2 + q_i^2)^{1/2}$, $\gamma_i = \tan^{-1}(q_i/p_i)$, with $i = r$ or s, the steady-state (fixed-point) solution and associated local stability are determined using the continuation approach. In the following (Figs. 4 and 5), solid lines indicate stable fixed points, whereas dashed (dotted) lines indicate unstable fixed points due to a saddle-node SN or pitchfork PF (Hopf, HF) bifurcation. The latter (HF) plays a significant role in the onset of periodic, quasi-periodic and chaotic responses, which will be checked through direct numerical integration results with proper initial conditions. For the sake of comparison, we assign $\mu_r = 0.005$, $\mu_s = 0.006$, $\sigma = 0$ in all cases, and consider $F = 0.005$ in frequency-response (FR) diagrams.

FR curves of cable A are shown in Fig. 4a, whereas the associated forcing amplitude-response (FAR) curves with $\sigma_f = 0.025$ are shown in Fig. 4b. In turn, FR curves of cables C and E are shown in Figs. 5a and b, respectively. Apart from overall quantitative differences, all nonlinear response diagrams manifest a general qualitative agreement as regards the coupled-mode ($a_r \neq 0$, $a_s \neq 0$) solution originating from the uncoupled-mode ($a_r = 0$, $a_s \neq 0$) one via a PF bifurcation, even though the type of the latter may be different, namely super-critical and/or sub-critical, thus giving rise to a stable and/or unstable coupled-mode solution. Yet, some meaningful differences are observed:

(i) Uncoupled-mode FR curves of cables A (Fig. 4a) and C (Fig. 5a) exhibit a hardening nonlinear behavior, whereas those of cable E (Fig. 5b) exhibit a softening nonlinear behavior similar to low-extensible

Table 3
A comparison of effective nonlinear coefficients of different primary/secondary crossover cables

Coefficients	Crossover cable		
	A	C	E
K_{rr}	−88,008.100	144,462.495	−31,366.931
K_{ss}	−90,803.684	−2,037,330.156	9857.837
K_{rs}	22,022.335	538,886.724	17,924.739
K	48,452.827	810,408.833	7283.243

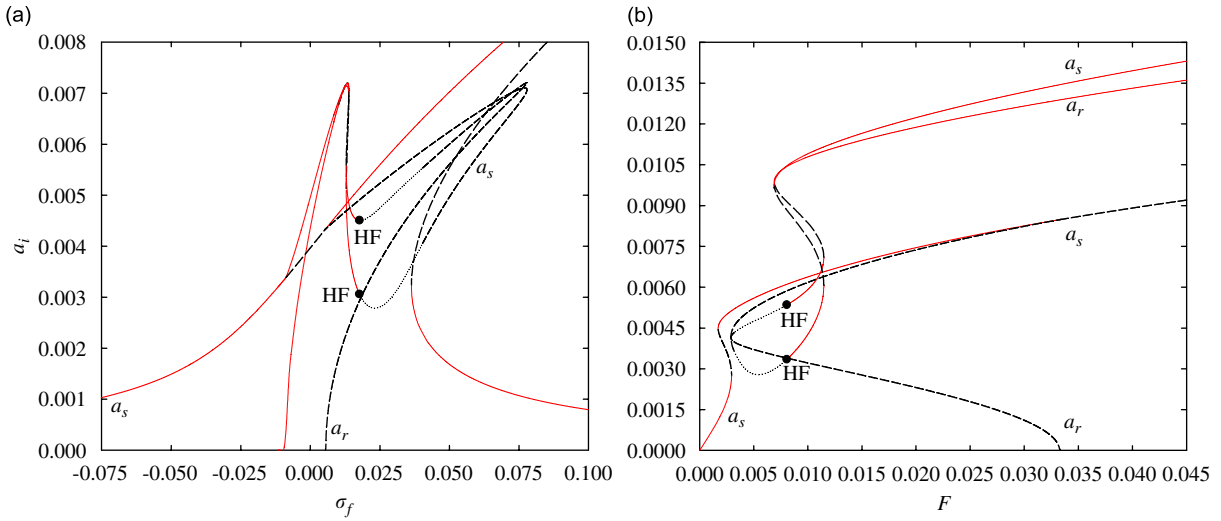

Fig. 4. (a) FR and (b) FAR curves and bifurcations of 1:1 resonant cable A involving longitudinal/transversal modal interaction.

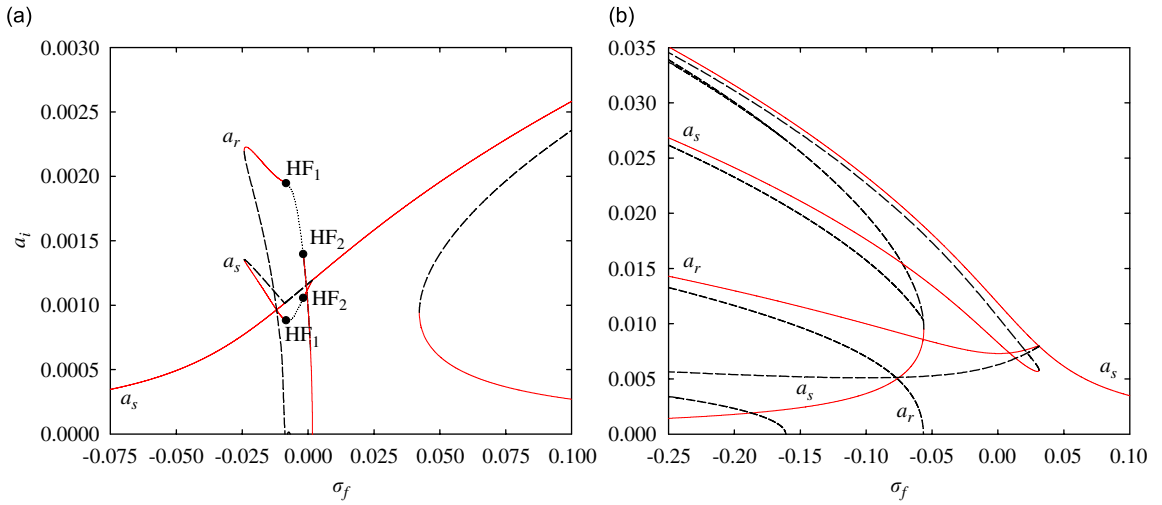

Fig. 5. FR curves and bifurcations of 1:1 resonant cables (a) C and (b) E involving longitudinal/transversal and transversal/transversal modal interaction, respectively.

suspended cables [8]. This is likely due to the sign difference in the associated coefficient K_{ss} (Table 3) entering Eqs. (6) and (7).

(ii) For cable E, up to seven (two stable and one unstable uncoupled, one stable and three unstable coupled) FR solutions are possible, with a coupled stable solution persisting over a wide σ_f range [8]. On the contrary, for both cables A and C, which exhibit a smaller number of solutions, the single coupled stable FR solution occurs in only a marginal σ_f range. Yet, multiple coupled stable solutions are possible in the relevant FAR curves (e.g., in Fig. 4b of cable A with $F = 0.01$).

Besides exhibiting typical SN and PF bifurcations, coupled-mode responses of cable A or C highlight one or two HF bifurcations, respectively, whereas those of cable E reveal none of them. This entails possible occurrence of periodic, quasi-periodic as well as chaotic oscillations for cables A and C involving longitudinal/transversal modal interactions. To verify such prediction, numerical transient-free time responses manifesting amplitude modulation are illustrated as follows.

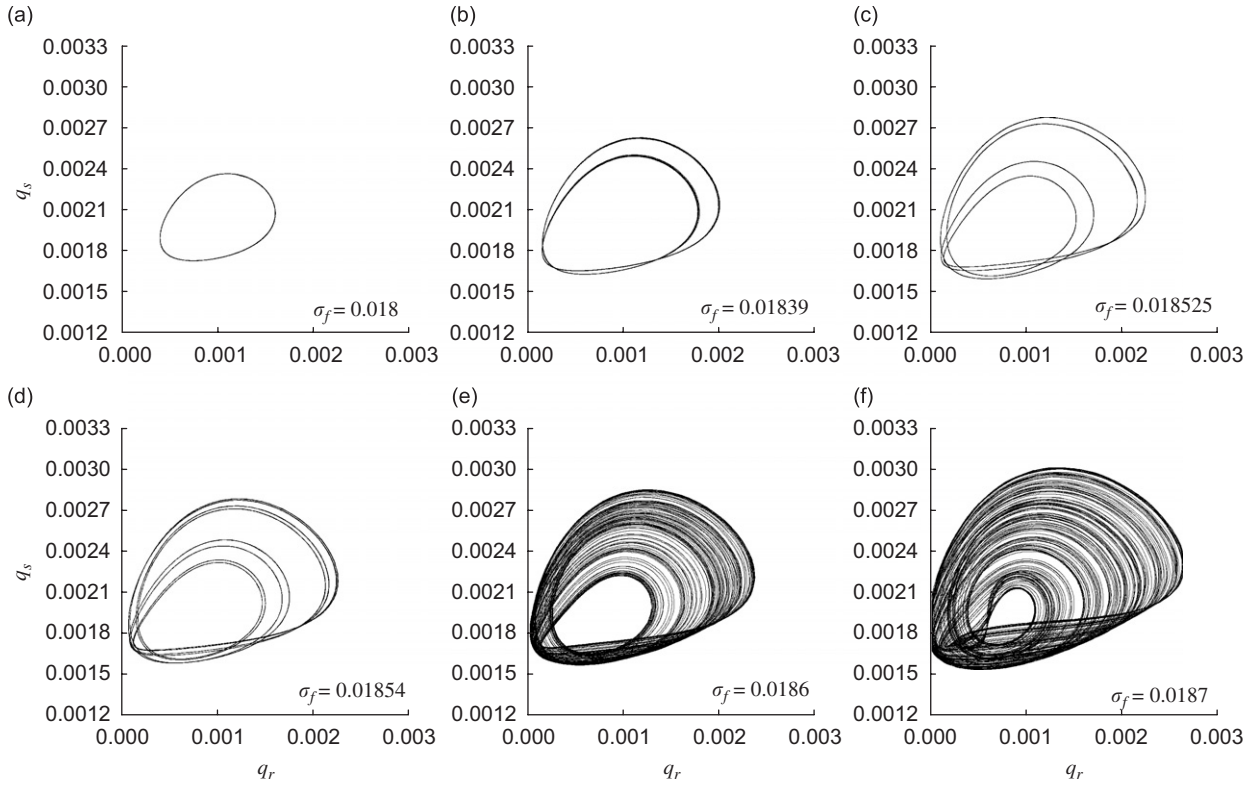

Fig. 6. A period doubling sequence leading to chaos due to longitudinal/transversal modal interaction of cable A.

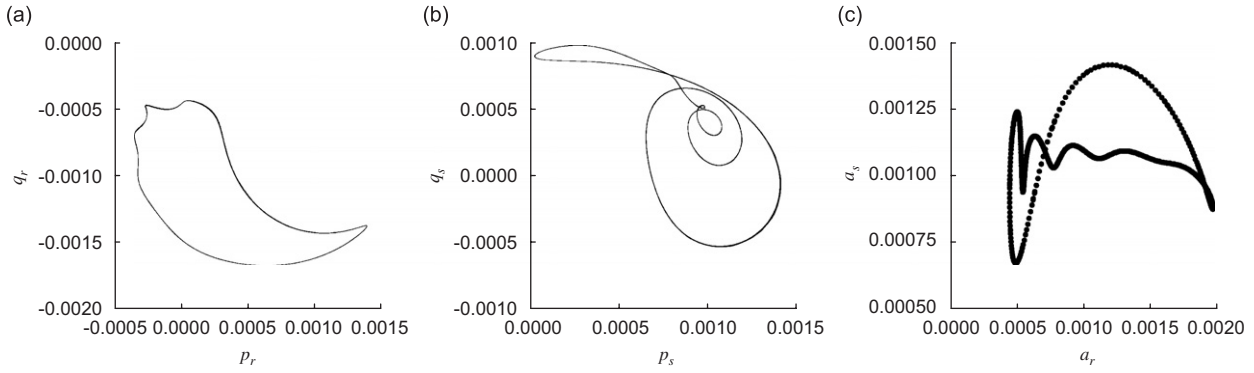

Fig. 7. A quasi-periodic motion due to longitudinal/transversal modal interaction of cable C.

Following the HF bifurcation ($\sigma_f \approx 0.0177$) in Fig. 4a, the q_r–q_s phase projection results with a slow increment in σ_f ($\sigma_f = 0.0180 \rightarrow 0.0187$) and fixed initial conditions are displayed in Fig. 6. The limit cycle (Fig. 6a) initially loses stability via a period-doubling bifurcation (Fig. 6b), leading to a progression of multiple closed-loop trajectories whose amplitudes considerably increase in size (Figs. 6c and d). Eventually, due to the accumulation of period doublings, the time histories appear aperiodic and the trajectories experience chaos as shown in Figs. 6e and f. By varying F, another chaotic oscillation is detected near the single HF bifurcation in the associated FAR curves in Fig. 4b. In turn, the occurrence of quasi-periodic response is exemplified in Fig. 7, corresponding to the FR curves in Fig. 5a with $\sigma_f \approx -0.006$ between the two HF bifurcations. Besides

showing different multi-harmonic features of p_r–q_r (Fig. 7a) and p_s–q_s (Fig. 7b) phase planes, a closed-loop map of a_r–a_s Poincarè section in Fig. 7c confirms a quasi-periodic motion.

Depending on coupled/uncoupled amplitudes, a comparison of space–time evolution of nonlinear longitudinal/transversal (u/v) displacements and dynamic tension T_d [8] over a half-forcing period is illustrated in Fig. 8. The T_d values are normalized with respect to the cable maximum static tension T_H at supports. The responses relevant to three coexisting (a_r,a_s) stable solutions, i.e., (0.010792, 0.010905), (0, 0.006378) and (0.005915, 0.004266) in Fig. 4b at $F = 0.01$, are illustrated in Fig. 8a–c, d–f and g–i, respectively. Overall, due to 1:1 resonant interaction at secondary crossover A (Fig. 1b), the spatial symmetric/anti-symmetric (anti-symmetric/symmetric) combination of longitudinal (transversal) configurations (Fig. 2), taking into account also second-order spatial corrections [12], highlights asymmetric features of time-varying $u(v)$ profiles in Fig. 8a or g (8b or h), whereas the uncoupled configurations preserve the spatially symmetric character of the directly excited v mode (Fig. 8e) accompanied by anti-symmetric u component (Fig. 8d). The resonantly coupled u and v configurations have comparable amplitudes, with the former (Fig. 8a or g) predominating over the latter (Fig. 8b or h) in the nonlinear range. This is clearly different from the associated uncoupled case (Fig. 8e vs. d) or from other resonant cases with transversal modal interactions in low-extensible cables at primary crossovers [8], whose v components are the only significant responses. Besides manifesting the spatially asymmetric character, the internally resonant-induced dynamic tensile or compressive forces—involving longitudinal/transversal modal interactions—are also substantially large due

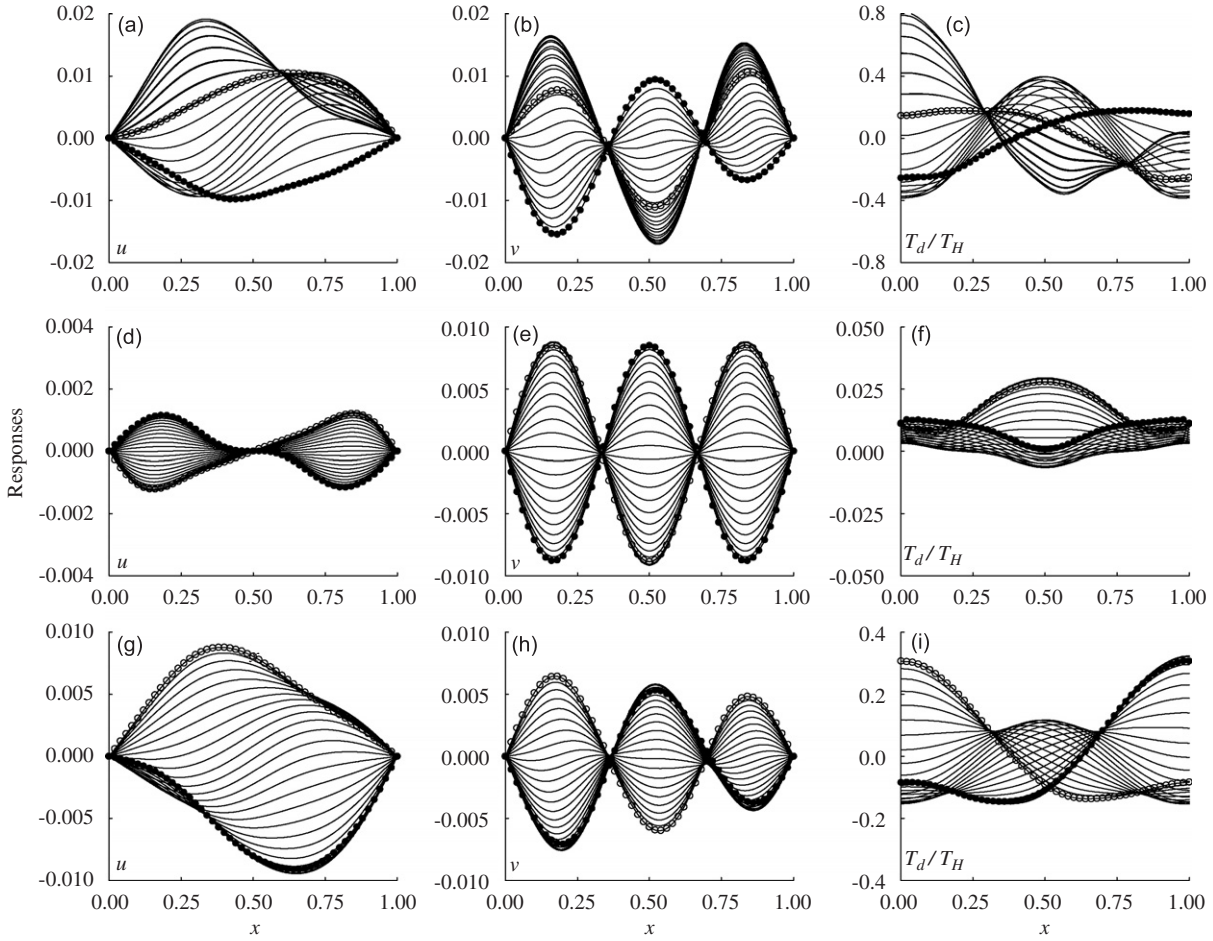

Fig. 8. A comparison of space–time varying u, v displacements and dynamic tensions (T_d/T_H) over a half-forcing period of multiple solutions in Fig. 4b with $F = 0.01$: (a_r,a_s) = (0.010792, 0.010905), (0, 0.006378) and (0.005915, 0.004266) for Fig. 8a–c, d–f and g–i, respectively; empty (filled) circles denote initial (final) results.

to both u and v contributions (Fig. 8c and i), with respect to the small-amplitude symmetric ones practically due to the predominant v contribution (Fig. 8f). The former figures highlight the importance of accounting for the longitudinal inertia ($\ddot{u}$) and the corresponding higher-order displacement gradients $\left(u'^2, u'^3\right)$, some of which being coupled with the transversal component $\left(u'^2 v'\right)$ [8].

Finally, it should be noted that the presented results are simply aimed at qualitatively evaluating the geometrical nonlinear (strain-displacement) effect on the finite-amplitude forced dynamics of highly (vs. lower) extensible cables. In this respect, the circumstance that some values of the elasto-geometric parameter λ/π possibly correspond to about the lower threshold of the physically admissible elastic range [3], in view of presently available values of the strength-to-stiffness material ratio, does not deserve special attention. On the other hand, considering a more realistic nonlinear and/or hysteretic constitutive (stress–strain) relationship (e.g., Refs. [5,10,16]) would be of major practical significance, and is left for future investigation.

5. Conclusions

Analysis of second-order geometrically quadratic nonlinear coefficients governing planar 1:1 resonant interactions of highly extensible suspended cables has highlighted meaningful higher-order longitudinal modal contributions at both primary/secondary frequency crossovers. By focusing on the secondary crossover cable involving the first longitudinal (i.e., elastic) mode, relevant *longitudinal/transversal* modal interactions provide some insights into the nonlinear dynamics of *highly extensible* cables, with respect to the primary crossover cable involving transversal/transversal modal interactions, whose response characteristics appear quite similar to those of low-extensible crossover cables [8]. In particular, the occurrence of periodic, quasi-periodic as well as chaotic oscillations involving the resonant longitudinal mode is revealed. Based on the effective quadratic/cubic nonlinearities, overall analytical–numerical outcomes, involving coupled longitudinal/transversal amplitudes, manifest space–time, multimodal, asymmetrical distributions of displacement and tension. These highlight a crucial role played, for even small-sagged suspended cables, by the *longitudinal inertia* and the associated higher-order displacement coupling accounted for through the underlying kinematic non-condensed modeling.

Acknowledgement

The first author wishes to acknowledge the *Postdoctoral Fellowship* from SAPIENZA University of Rome.

References

[1] J.J. Burgess, M.S. Triantafyllou, The elastic frequencies of cables, *Journal of Sound and Vibration* 120 (1988) 153–165.
[2] M. Al-Qassab, S. Nair, Wavelet-Galerkin method for free vibrations of elastic cable, *ASCE Journal of Engineering Mechanics* 129 (2003) 350–357.
[3] W. Lacarbonara, A. Paolone, F. Vestroni, Elastodynamics of non-shallow suspended cables: linear modal properties, *ASME Journal of Vibration and Acoustics* 129 (2007) 425–433.
[4] H.P. Lin, N.C. Perkins, Free vibration of complex cable/mass systems: theory and experiment, *Journal of Sound and Vibration* 179 (1995) 131–149.
[5] M.S. Triantafyllou, D.K.P. Yue, Damping amplification in highly extensible hysteretic cables, *Journal of Sound and Vibration* 186 (1995) 355–368.
[6] G. Rega, Nonlinear dynamics of suspended cables, Part I: Modeling and analysis and Part II: Deterministic phenomena, *ASME Applied Mechanics Review* 57 (2004) 443–514.
[7] H.M. Irvine, T.K. Caughey, The linear theory of free vibrations of a suspended cable, *Proceeding of the Royal Society of London Series A* 341 (1974) 229–315.
[8] N. Srinil, G. Rega, The effects of kinematic condensation on internally resonant forced vibrations of shallow horizontal cables, *International Journal of Non-Linear Mechanics* 42 (2007) 180–195.
[9] B.L. Newberry, N.C. Perkins, Investigation of resonant tensioning in submerged cables subjected to lateral excitation, *International Journal of Offshore and Polar Engineering* 7 (1997) 48–53.
[10] A.A. Tjavaras, Q. Zhu, Y. Liu, M.S. Triantafyllou, D.K.P. Yue, The mechanics of highly-extensible cables, *Journal of Sound and Vibration* 213 (1998) 709–737.

[11] N. Srinil, G. Rega, Two-to-one resonant multi-modal dynamics of horizontal/inclined cables, Part II: Internal resonance activation, reduced-order models and nonlinear normal modes, *Nonlinear Dynamics* 48 (2007) 253–274.
[12] N. Srinil, G. Rega, S. Chucheepsakul, Two-to-one resonant multi-modal dynamics of horizontal/inclined cables, Part I: Theoretical formulation and model validation, *Nonlinear Dynamics* 48 (2007) 231–252.
[13] N. Srinil, R. Alaggio, G. Rega, Experimental linear/nonlinear dynamics of an extensible sagged inclined cable, *Proceedings of the Seventh International Symposium on Cable Dynamics*, Vienna, Austria, 2007, to appear.
[14] G. Rega, N. Srinil, Nonlinear hybrid-mode resonant forced oscillations of sagged inclined cables at avoidances, *ASME Journal of Computational and Nonlinear Dynamics* 2 (2007) 324–336.
[15] G. Rega, W. Lacarbonara, A.H. Nayfeh, Reduction methods for nonlinear vibrations of spatially continuous systems with initial curvature, *IUTAM Symposium on Recent Developments in Nonlinear Oscillations of Mechanical Systems*, in: Nguyen Van Dao, E.J. Kreuzer (Eds.), *Solid Mechanics and Its Applications*, Vol. 77, Kluwer, Dordrecht, 2000, pp. 235–246.
[16] M.J. Leamy, O. Gottlieb, Internal resonances in whirling strings involving longitudinal dynamics and material non-linearities, *Journal of Sound and Vibration* 236 (2000) 683–703.